HHS Public Access

Author manuscript

Nanoscale Horiz. Author manuscript; available in PMC 2024 November 20.

Published in final edited form as:

Nanoscale Horiz. ; 8(12): 1677–1685. doi:10.1039/d3nh00365e.

Pneumatic nano-sieve for CRISPR-based detection of drug-resistant bacteria†

Ruonan Peng[‡,a], **Xinye Chen**[‡,a,b], **Fengjun Xu**[a], **Richard Hailstone**[c], **Yujie Men**[a], **Ke Du**[a]

[a] Department of Chemical and Environmental Engineering, University of California, Riverside, 900 University Ave, Riverside, CA 92507, USA.

[b] Department of Microsystems Engineering, Rochester Institute of Technology, 1 Lomb Memorial Dr, Rochester, NY 14623, USA.

[c] Center for Imaging Science, Rochester Institute of Technology, 1 Lomb Memorial Dr, Rochester, NY 14623, USA.

Abstract

The increasing prevalence of antibiotic-resistant bacterial infections, particularly methicillin-resistant *Staphylococcus aureus* (MRSA), presents a significant public health concern. Timely detection of MRSA is crucial to enable prompt medical intervention, limit its spread, and reduce antimicrobial resistance. Here, we introduce a miniaturized nano-sieve device featuring a pneumatically-regulated chamber for highly efficient MRSA purification from human plasma samples. By using packed magnetic beads as a filter and leveraging the deformability of the nano-sieve channel, we achieved an on-chip concentration factor of ~ 15-fold for MRSA. We integrated this device with recombinase polymerase amplification (RPA) and clustered regularly interspaced short palindromic repeats (CRISPR)-Cas detection system, resulting in an on-chip limit of detection (LOD) of approximately 100 CFU/mL. This developed approach provides a rapid, precise, and centrifuge-free solution suitable for point-of-care diagnostics, with the potential to significantly improve patient outcomes in resource-limited medical conditions.

Graphical Abstract

†Electronic Supplementary Information (ESI) available. See DOI: 00.0000/00000000.

ke.du@ucr.edu .

‡These authors contributed equally to this work.

Author Contributions

Ruonan Peng, Xinye Chen and Ke Du designed the experiments. Ruonan Peng, Xinye Chen, Richard Hailstone, and Fengjun Xu performed the experiments. Ruonan Peng and Xinye Chen wrote the manuscript. All authors commented the manuscript.

Conflicts of interest

There are no conflicts to declare.

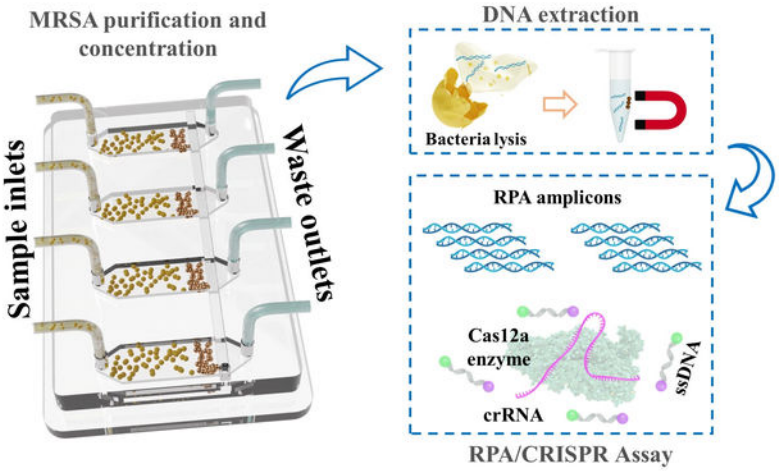

Introduction

The prevalence of antibiotic-resistant bacterial infections has become a major concern for both individuals and healthcare facilities, causing an estimated 1.27 million fatalities globally and contributing to nearly 5 million deaths in 2019[1]. One particular pathogen, methicillin-resistant *Staphylococcus aureus* (MRSA), stands out as a prominent multidrug-resistant (MDR) bacterium that presents a serious challenge[2]. MRSA can cause skin infections[3], pneumonia[4] and even sepsis[5], and it exhibits resistance to beta-lactam antibiotics, including methicillin, penicillin, amoxicillin, and oxacillin, which are commonly used in the treatment of bacterial infections[6]. Consequently, infections caused by MRSA are associated with high morbidity and mortality rates, making it a significant public health issue[7].

Early detection of MRSA is crucial as it enables timely and appropriate medical intervention, prevents the spread of these pathogens, and reduces the risk of antimicrobial resistance[8]. For detection, it is essential to isolate bacteria from the samples collected from nose[9], blood[10] or urine[11]. Membrane-based filtration is a widely used and advantageous method for capturing bacteria due to its cost-effectiveness, simplicity, and rapidness[12]. Furthermore, a significant challenge associated with this technique is the extensive volume of iterative washing buffer required to retrieve the captured bacteria from the membrane[13]. This washing process can inadvertently lead to dilution of the captured bacteria, reducing their concentration to levels that may fall below the detection limit of downstream detection processes. Alternatively, microfluidic platforms have emerged as a powerful tool in the field of bacterial purification and concentration[14,15]. Those platforms could be functionalized to rapidly and efficiently separate and concentrate target bacteria, depending on various working principles, including inertial force[16,17], hydrodynamics[18,19], electrophoresis[20,21], and acoustics[22,23]. However, these techniques require either complicated fabrication processes or extra laboratory-based instruments, increasing the complexity of microfluidic platforms for delicate operations. Therefore, it is important to develop a simple and direct

process of fabricating a microfluidic platform while ensuring it can effectively separate the target bacteria.

Traditional MRSA detection methods, such as cultured-based techniques, are time-consuming and labor-intensive. Molecular methods like polymerase chain reaction (PCR) require thermocyclers and sophisticated bulky equipment, which renders them unsuitable for resource-limited point-of-care (POC) environments[24]. Clustered regularly interspaced short palindromic repeats (CRISPR)-Cas (CRISPR-associated) systems, particularly the Cas12 and Cas13 nucleases, have gained significant attention in the field of in vitro diagnostics[25]. Among them, Cas12a relies solely on a complementary crRNA for targeting specific DNA sequences and utilizes a single RuvC domain to cut the target DNA, a process known as cis-cleavage[26,27]. Moreover, Cas12a exhibits collateral activity, referred to as trans-cleavage, which allows it to non-specifically cleave neighboring single-stranded DNAs (ssDNA) following target binding[28]. To exploit this feature for detection purposes, ssDNA can be labeled with a fluorophore-quencher, and upon Cas12a activation through target binding, the cleavage of ssDNA generates an increase in fluorescence signal[29]. CRISPR-Cas12a system operates at 37°C, making it more suitable for POC detection than traditional PCR methods[30]. Additionally, by combining the CRISPR-Cas system with isothermal amplification methods such as recombinase polymerase amplification (RPA)[31], rolling circle amplification[32] (RCA), and loop-mediated isothermal amplification (LAMP)[33], the specificity and sensitivity of CRISPR-Cas detection can be further enhanced in POC settings[34]. Notably, RPA stands out as a widely adopted amplification method due to its simplicity, rapidity, and compatibility with the same temperature requirements as CRISPR assays.

Herein, we introduce a miniaturized and versatile nano-sieve device with a pneumatically-regulated chamber that allows for rapid purification and highly concentrated isolation of MRSA from plasma samples. To achieve this, we developed a simplified, direct, and cost-efficient fabrication process for this nano-sieve device, incorporating multiple channels. With a three-dimensional (3-D) magnetic beads-stacked microstructure within the channel, the highly efficient bacteria capture was preceded by precisely controlling the applied flow rate. Leveraging the deformability of the nano-sieve channel, a remarkable concentration (around 15-fold) of captured bacteria was achieved by adjusting the volume ratio of initial sample solution and retrieved buffer solution. This unique functionality of nano-sieve significantly enhances the limit of detection (LOD) when combined with the developed RPA and CRISPR-Cas assay, ultimately achieving an on-chip LOD of approximately 100 CFU/mL. Importantly, the entire process can be completed in less than 4 hours under physiological temperature and room temperature, without the need of centrifugation. Therefore, our approach of integrating the microfluidic-based multiplexing purification and a rapid and precise molecular detection could potentially improve the sensitivity and specificity of MRSA detection.

Results and Discussion

The schematic of the whole system is presented in Fig. 1a, where multiple nano-sieve channels are designed for multiplexing separation of bacteria from initial samples. Fig. 1b

shows the picture of a practical nano-sieve device, including the beads-stacked channel filled with blue food dye and the pneumatic layer filled with red food dye. This indicates the device can be successfully fabricated without any leaking issues. In Fig. 1c, the fabrication flow of a pneumatically-regulated nano-sieve device is exhibited. It started with a thin layer of TEOS (200 nm in thickness) deposited onto a pre-cleaned glass wafer, which was followed by a spin-coated layer of positive photoresist. After that, a pattern of nano-sieve channel was transferred from a plastic photomask to the photoresist layer by photolithography technique, then defined on the layer of TEOS by BOE process. The patterned channel with a thickness of 200 nm was created, and finally covered by a thin layer of positive photoresist as a sacrificial support for PDMS bonding procedure. This coated photoresist can eliminate the technical issue of collapsed PDMS roof[35], significantly enhancing the fabrication of nano-fluidic channels. The pneumatic chamber was made by employing a 3-D printed mold, and a thin film of uncured PDMS was sandwiched by glass slides, with a supporting ORACAL film to define the thickness of this PDMS film to be created. Then the pneumatic chamber and the cured PDMS thin film were bonded through the plasma treatment. The fabrication of the nano-sieve device was subsequently completed by bonding the pneumatic chamber layer and the glass substrate patterned with nano-sieve channels via plasma treatment. Both treatments (marked by the red dashed rectangles) were followed by the baking process on a hot plate to achieve the strong bonding in between.

The pre-loaded stacked beads array within the half section of the nano-sieve channel is displayed in the optical micrograph in Fig. 2a, which are well secured by the positive pressure applied in the pneumatic chamber. Another half section per channel was connected to the outlets for collecting the waste liquids. Fig. 2b presents the experimental setup, regarding a multiplexing separation of target bacteria under the observation of fluorescence microscopy. Within these nano-sieve channels as shown in Fig. 2c, only the target bacteria stained by the green dye can display the green fluorescent signals. During the flow condition, the bacteria were carried by flowing fluid, moving forward to the area of stacked beads, where they were physically captured by the array of 5 μm beads. It is noticed that the ratio of MRSA bacteria to the magnetic beads is very low without saturation problems. As shown in Fig. 2d and Fig. 2e, the original bacterial sample and retrieved bacterial sample were compared to highlight the on-chip concentration capability of this powerful nano-sieve system. The retrieved bacteria sample shows higher concentration of target bacteria than the original bacteria sample that has a lower concentration. Due to the pure physical process, there is no on-chip culturing involved through the MRSA purification.

After successfully concentrating MRSA using nano-sieve, standard plate count was employed to quantify the concentration ability of nano-sieve. Table 1 displays the concentration factors achieved with various inlet concentrations using the nano-sieve device. The concentration factor was determined by dividing the inlet concentration by the outlet concentration. A total of 600 μL of MRSA was injected into inlets, while 30 μL of PBS was used to retrieve the MRSA, resulting in a theoretical concentration factor of 20. However, as the MRSA concentration increased, the experimental concentration factor slightly decreased. One possible reason for this is that some bacteria may have leaked out through the waste outlets due to the increase in MRSA concentration. This suggests that the nano-sieve is

more suitable for concentrating low-concentration bacteria, aligning with our objective of enhancing the detection limit.

The nucleic acid purification process using magnet beads after the MRSA lysis is shown in Fig. 3a. In this process, magnet beads are introduced into a solution containing DNA, wherein a substantial amount of salt and polyethylene glycol (PEG) is present[36]. The DNA molecules become crowded out and bind to the surface of the beads through electrostatic interactions[37] and molecular crowding[38]. Magnet fields are then applied to collect DNA-bound beads, effectively removing unwanted debris such as membrane lipids and proteins[39]. Then, guanidinium chloride is utilized to wash DNA as it disrupts protein-DNA interactions and aids in solubilizing and denaturing proteins[40]. Finally, purified DNA is eluted using nuclease-free water. Fig. 3b shows the mechanism of RPA amplification. This process relies on the coordinated activities of recombinases, single-stranded DNA-binding proteins, and DNA polymerases to achieve isothermal amplification of the target DNA. The reaction is initiated by recombinases facilitating the binding of primers to the target DNA sequence. Single-stranded DNA-binding proteins stabilize the displaced DNA strands, allowing DNA polymerases to efficiently extend the primers along the DNA template in the presence of deoxynucleotide triphosphates (dNTPs), resulting in the synthesis of new DNA strands. Following this, the RPA amplicons are introduced into the CRISPR-Cas12a reaction. As shown in Fig. 3c, in positive samples, when the Cas12a-crRNA complex encounters the complementary target DNA, it undergoes a conformational change, leading to the activation of its nuclease activity. Cas12a then cleaves the target DNA at a specific site (cis-cleavage) as well as the collateral ssDNA probes (trans-cleavage), leading to the release of fluorescence signals from the fluorophore. In negative samples lacking the target DNA, the nuclease activity of Cas12a remains inactivated, preventing the cleavage of the probe and the generation of fluorescence signals.

The assay development started with primer screening. Two CRISPR RNA and four primers sets were chosen, and their sequences are listed in Table S1 (ESI†). The input DNA was extracted from 10^8 CFU/mL MRSA and purified using magnet beads. The excitation and emission wavelengths were set at 480 nm and 520 nm, respectively. The results of the primer screening are depicted in Fig. 4a. With the preceding RPA amplification, the fluorescence signal exhibited a substantial increase in comparison to CRISPR-Cas12a detection performed without RPA. Among the groups, the combination of crRNA2 and primer set 4 demonstrated the highest fluorescence signal, thus being chosen for subsequent experiments. To further evaluate the assay performance, a comparison was made between the magnet beads purification and a scenario without such purification. The results revealed a significant reduction in fluorescence signal without magnet beads purification, as illustrated in Fig. 4b. One possible explanation is that the presence of EDTA, lysosome, and proteinase K, which were introduced during MRSA lysis, might have disrupted the enzyme system, ultimately leading to the failure of DNA amplification and detection. On the other hand, magnetic beads purification effectively eliminated unwanted debris, including lysosome and proteinase K, thereby ensuring the successful amplification and detection of the target DNA. Fig. 4c displays the TEM images of magnet beads only (top) and magnet beads plus DNA (bottom). In the top image, aggregation and clustering of the beads can be observed, while the bottom image demonstrates the binding of DNA molecules to the

magnet beads through electrostatic interactions and molecular crowding. Furthermore, the specificity performance of the assay was evaluated using three additional strains: wild-type *E. coli* K12 (Fig. 4d), kanamycin-resistant *E. coli* K12 (Fig. 4e), and wild-type *S. aureus* (Fig. 4f). The input DNA was extracted from bacterial cultures with a concentration of 10^8 CFU/mL. The PBS buffer solution lacking bacteria was served as no template control (NTC). The results show that the fluorescence signals generated by these bacteria were comparable to that of the NTC group. However, upon mixing these bacteria with MRSA at a ratio of 1:1, the fluorescence signal of the mixture significantly increased. Particularly, the fluorescence signal produced by wild-type S. aureus reached nearly the same level as that in pure MRSA. These results not only confirm the specificity of the assay but also suggest that the presence of other bacteria does not interfere with MRSA detection results.

Fig. 5a presents a comparison of fluorescence signal obtained from off-chip and on-chip detection, encompassing various inlet MRSA concentrations ranging from 10^4 CFU/mL to 10^6 CFU/mL. When the MRSA concentration reached 10^6 CFU/mL, both the on-chip and off-chip results exhibited saturation in fluorescence signal. As the MRSA concentrations decreased, the off-chip results displayed a decline in fluorescence signal, whereas the onchip results remained saturated. Notably, at an MRSA concentration of 10^4 CFU/mL, a discernible difference in fluorescence signal between the on-chip and off-chip results became evident, as depicted in Fig. 5b. Subsequently, the on-chip detection limit was determined by further decreasing the MRSA concentration. Fig. 5c presents the fluorescence signal acquired from on-chip detection using inlet MRSA concentrations ranging from 10 CFU/mL to 10^3 CFU/mL, accompanied by the corresponding endpoint images displayed in Fig. 5d. At an MRSA concentration of 100 CFU/mL, the naked eye easily discerned the fluorescence differences between the positive and negative groups, which were further validated through one-way ANOVA analysis of quantified characterization[41]. The presence of two asterisks between the 100 CFU/mL group and NTC indicates a statistically significant difference, stating that our assay can reliably detect MRSA at a concentration of 100 CFU/mL. On the other hand, the ‘ns’ (non-significant) result between the 10 CFU/mL group and NTC explains that the fluorescence signals from these two groups are not significantly different, which states that detection limit of our assay lies somewhere between 10 CFU/mL and 100 CFU/mL. Therefore, a detection limit of 100 CFU/mL was established for MRSA detection using the nano-sieve device.

The approach of rapidly purifying and highly concentrating pathogens from a large volume of bodily fluids could be crucial for disease diagnostics, such as sepsis, at the early stage[42,43]. Compared to the surface chemistry technique, pathogen separation based on the physical structure of microfluidic platforms could be simpler and more efficient, while minimizing contamination issues. Compared to filter membranes, our device only needs a small amount of buffer solution to collect and concentrate the trapped bacteria to extend the detection limit. The concentration factor could be further improved by adjusting the volume ratio of initial sample solution and buffer solution. Our nano-sieve system has been functionalized via a 3-D beads-stacked microstructure that can be precisely tuned by applied flow rate[44], and optimized via a pneumatic layer that can counterbalance the hydrodynamic pressure during the flow condition[45]. Moreover, our pneumatically-regulated nano-sieve has been developed with an extremely low aspect ratio of 1:25,000, significantly

reducing the hydrodynamic pressure that may affect the mechanically-driven separation process. This flexible pneumatic layer enhances the adaptability of our nano-sieve channel compared to a rigid nanofluidic channel. Therefore, this deformable pneumatic layer enables a more reliable bead-stacking by applying the positive air pressure during the purification process and an easier target release by offering the negative air pressure during the retrieval process. In addition, we recently showed that the pneumatic-controlled nano-sieve with a patterned microstructure on the bottom of the substrate could efficiently enhance the capture of nanoscale targets at a higher flow rate[45]. In the future, the development of 3-D spaced beads array, such as a combination of various sized beads, could be beneficial to a higher capture efficiency of target bacteria, aiming to improve the detection limit by combining with our optimized molecular detection technique. While our current study involved spiking MRSA into plasma samples, future research will focus on testing clinical samples to validate the applicability of our approach in a real-world clinical setting. Currently, our group is engaged in the development of a rapid and efficient method for purifying and identifying antibiotic-resistant bacteria (ARB) from human blood samples. Through an immunomagnetic assay, highly concentrated red blood cells (RBCs) could be removed from bacteria-spiked samples, while effectively retaining the target bacteria for subsequent purification using the optimized nano-sieve device. Presently, our system only processes up to six samples simultaneously, but by introducing more channels during the chip fabrication process, we can achieve the simultaneous detection of hundreds of clinical samples within a 6-inch wafer using a simple equipment setup comprising a multipump, pipetting system, heat block, magnet, transilluminator, and necessary reagents. To prevent the samples from being contaminated, the initial samples were loaded in the single-used and sterilized syringe, then pumped through the sterilized microfluidic tubing into each independent channel that was filled with the beads stacking. Consequently, the entire environment is closed and sterilized for target bacteria purification, and there is no contact between the equipment and the applied sample. Such high-throughput capability will significantly reduce the turnaround time for patients and healthcare providers to obtain the test results, which is crucial for expediting disease diagnosis, facilitating prompt medical interventions, and ensuring timely implementation of appropriate treatment strategies[46]. This pneumatically-regulated nano-sieve device was designed and fabricated as a cost-effective and disposable system for POC applications without recycling concerns. The MRSA purification process is entirely based on silica microbeads stacking within the channels of device. This entire chip could be stored in environmental conditions for an extended duration, making it well-suited for sample preparation for POC setting. Additionally, one novelty of our approach is centrifuge-free DNA extraction by using the immunomagnetic beads. This method not only facilitated our work with spiked plasma samples but also eliminated the need for centrifugation, which is superior to commercially available spin column extraction kits, which rely on complicated and expensive centrifuge processes. Our centrifuge-free method is more affordable and further cost reductions could be achieved by synthesizing our own DNA extraction beads. On the other hand, by designing different primers and CRISPR RNA, this microfluidic device enables multiplexing for different pathogens. This feature holds significant promise in the diagnosis of diseases potentially caused by multiple pathogens, such as sepsis[47]. While our detection assay is currently performed in tubes after the nano-sieve concentration, requiring manual pipetting, our future work will focus on the incorporation of a platform

for the detection assay, such as the funnel-adapted sensing tube (FAST)[48] or a digital multiplex dRPA chip[49]. Also, we could simplify the operation process by introducing a one-pot RPA and CRISPR assay[50]. By continuously optimizing our nano-sieve device and CRISPR assays, a higher sensitivity of our designed system could be achieved for a rapid and multiplexing detection of bloodborne and urine traction diseases.

Conclusion

In conclusion, we have introduced a miniaturized and versatile nano-sieve device with a pneumatically-regulated chamber for the rapid purification and highly concentrated isolation of MRSA from plasma samples. Our simplified and cost-efficient fabrication process, incorporating multiple channels and a 3D beads-stacked microstructure, enables highly efficient capture of MRSA by precisely controlling the flow rate, resulting in a significant concentration of captured bacteria. The integration of this device with RPA and CRISPR-Cas12 assay enhances the detection sensitivity, achieving a lower on-chip detection limit of 100 CFU/mL compared to the off-chip limit of 10^4 CFU/mL. Our sensitive detection method can be completed within a short timeframe of 4 hours under physiological temperature conditions, eliminating the need for centrifugation. The scalability of the nano-sieve device allows for the simultaneous processing of multiple clinical samples and multiplexing detection of different pathogens. By improving the sensitivity and specificity of MRSA detection, our approach holds promise in contributing to better patient outcomes and addressing the challenges posed by antibiotic-resistant bacterial infections.

Supplementary Material

Refer to Web version on PubMed Central for supplementary material.

Acknowledgements

This study was supported by The National Institutes of Health R35GM 142763.

References

1. Murray CJ, Ikuta KS, Sharara F, Swetschinski L, Aguilar GR, Gray A, Han C, Bisignano C, Rao P, Wool E et al., The Lancet, 2022, 399, 629–655.
2. Lee AS, De Lencastre H, Garau J, Kluytmans J, Malhotra-Kumar S, Peschel A and Harbarth S, Nature reviews Disease primers, 2018, 4, 1–23.
3. Formosa-Dague C, Fu Z-H, Feuillie C, Derclaye S, Foster TJ, Geoghegan JA and Dufrêne YF, Nanoscale Horizons, 2016, 1, 298–303. [PubMed: 32260649]
4. Rubinstein E, Kollef MH and Nathwani D, Clinical Infectious Diseases, 2008, 46, S378–S385. [PubMed: 18462093]
5. Jiang X, Wang Y, Qin Y, He W, Benlahrech A, Zhang Q, Jiang X, Lu Z, Ji G and Zheng Y, Scientific Reports, 2017, 7, 41964. [PubMed: 28165033]
6. Liu W-T, Chen E-Z, Yang L, Peng C, Wang Q, Xu Z and Chen D-Q, Microbial pathogenesis, 2021, 156, 104915. [PubMed: 33930416]
7. Cao M, Chang Z, Tan J, Wang X, Zhang P, Lin S, Liu J and Li A, ACS applied materials & interfaces, 2022, 14, 13025–13037. [PubMed: 35285619]
8. Palavecino EL, Methicillin-resistant Staphylococcus aureus (MRSA) protocols, 2014, 71–83.

9. Schulz M, Calabrese S, Hausladen F, Wurm H, Drossart D, Stock K, Sobieraj AM, Eichenseher F, Loessner MJ, Schmelcher M et al., Lab on a Chip, 2020, 20, 2549–2561. [PubMed: 32568322]
10. Fan Z, Khan SA, Dai X, Tchouwou C, Lu Y and Ray PC, Particle & Particle Systems Characterization, 2014, 31, 357–364.
11. Mahdiyoun SM, Kazemian H, Ahanjan M, Houri H and Goudarzi M, Jundishapur journal of microbiology, 2016, 9, e37238.
12. García-Fernández E, Koch G, Wagner RM, Fekete A, Stengel ST, Schneider J, Mielich-Süss B, Geibel S, Markert SM, Stigloher C et al., Cell, 2017, 171, 1354–1367. [PubMed: 29103614]
13. Nebe-von Caron G, Stephens P, Hewitt C, Powell J and Badley R, Journal of microbiological methods, 2000, 42, 97–114. [PubMed: 11000436]
14. Mach AJ and Di Carlo D, Biotechnology and bioengineering, 2010, 107, 302–311. [PubMed: 20589838]
15. Lee J-J, Jeong KJ, Hashimoto M, Kwon AH, Rwei A, Shankarappa SA, Tsui JH and Kohane DS, Nano letters, 2014, 14, 1–5. [PubMed: 23367876]
16. Narayana Iyengar S, Kumar T, Mårtensson G and Russom A, Electrophoresis, 2021, 42, 2538–2551. [PubMed: 34510466]
17. Condina MR, Dilmetz BA, Bazaz SR, Meneses J, Warkiani ME and Hoffmann P, Lab on a Chip, 2019, 19, 1961–1970. [PubMed: 31099359]
18. Herrmann N, Neubauer P and Birkholz M, Biomicrofluidics, 2019, 13, 061501. [PubMed: 31700559]
19. Bayareh M, Chemical Engineering and Processing-Process Intensification, 2020, 153, 107984.
20. Zhang Y, Zhu L, Zhang Y, He P and Wang Q, Journal of Chromatography A, 2018, 1555, 100–105. [PubMed: 29724645]
21. Podszun S, Vulto P, Heinz H, Hakenberg S, Hermann C, Hankemeier T and Urban GA, Lab on a Chip, 2012, 12, 451–457. [PubMed: 22008897]
22. Dow P, Kotz K, Gruszka S, Holder J and Fiering J, Lab on a Chip, 2018, 18, 923–932. [PubMed: 29445800]
23. Ohlsson P, Petersson K, Augustsson P and Laurell T, Scientific reports, 2018, 8, 9156. [PubMed: 29904138]
24. He J, Peng R, Yuqing H, Karim R, Chen J, Lu G and Du K, ACS Applied Materials & Interfaces, 2023.
25. Xu Z, Chen D, Li T, Yan J, Zhu J, He T, Hu R, Li Y, Yang Y and Liu M, Nature Communications, 2022, 13, 6480.
26. Zetsche B, Gootenberg JS, Abudayyeh OO, Slaymaker IM, Makarova KS, Essletzbichler P, Volz SE, Joung J, Van Der Oost J, Regev A et al., Cell, 2015, 163, 759–771. [PubMed: 26422227]
27. Li S-Y, Cheng Q-X, Liu J-K, Nie X-Q, Zhao G-P and Wang J, Cell research, 2018, 28, 491–493. [PubMed: 29531313]
28. Weng Z, You Z, Yang J, Mohammad N, Lin M, Wei Q, Gao X and Zhang Y, Angewandte Chemie International Edition, 2023, 62, e202214987. [PubMed: 36710268]
29. Kaminski MM, Abudayyeh OO, Gootenberg JS, Zhang F and Collins JJ, Nature Biomedical Engineering, 2021, 5, 643–656.
30. Gootenberg JS, Abudayyeh OO, Kellner MJ, Joung J, Collins JJ and Zhang F, Science, 2018, 360, 439–444. [PubMed: 29449508]
31. Kanitchinda S, Srisala J, Suebsing R, Prachumwat A and Chaijarasphong T, Biotechnology reports, 2020, 27, e00485. [PubMed: 32577410]
32. Qing M, Chen SL, Sun Z, Fan Y, Luo HQ and Li NB, Analytical Chemistry, 2021, 93, 7499–7507. [PubMed: 33980009]
33. Mukama O, Yuan T, He Z, Li Z, de Dieu Habimana J, Hussain M, Li W, Yi Z, Liang Q and Zeng L, Sensors and Actuators B: Chemical, 2020, 316, 128119.
34. Feng W, Zhang H and Le XC, Analytical Chemistry, 2023, 95, 206–217. [PubMed: 36625124]
35. Lee J, Yoon YK, Kim J, Kim Y and Jo K, Bulletin of the Korean Chemical Society, 2011, 32, 33–34.

36. Liu D, Li Q, Luo J, Huang Q and Zhang Y, BMC genomics, 2023, 24, 125. [PubMed: 36927488]
37. Haddad Y, Xhaxhiu K, Kopel P, Hynek D, Zitka O and Adam V, International Journal of Molecular Sciences, 2016, 17, 550. [PubMed: 27104527]
38. Oberacker P, Stepper P, Bond DM, Höhn S, Focken J, Meyer V, Schelle L, Sugrue VJ, Jeunen G-J, Moser T et al., PLoS biology, 2019, 17, e3000107. [PubMed: 30629605]
39. Tang C, He Z, Liu H, Xu Y, Huang H, Yang G, Xiao Z, Li S, Liu H, Deng Y et al., Journal of Nanobiotechnology, 2020, 18, 1–19. [PubMed: 31898555]
40. Macdonald RD and Khajehpour M, Biophysical chemistry, 2015, 196, 25–32. [PubMed: 25268875]
41. Kim TK, Korean journal of anesthesiology, 2017, 70, 22–26. [PubMed: 28184262]
42. Fang Y-L, Wang C-H, Chen Y-S, Chien C-C, Kuo F-C, You H-L, Lee MS and Lee G-B, Lab on a Chip, 2021, 21, 113–121. [PubMed: 33232424]
43. Ohlsson P, Evander M, Petersson K, Mellhammar L, Lehmusvuori A, Karhunen U, Soikkeli M, Seppa T, Tuunainen E, Spangar A et al., Analytical chemistry, 2016, 88, 9403–9411. [PubMed: 27264110]
44. Chen X, Miller A, Cao S, Gan Y, Zhang J, He Q, Wang R-Q, Yong X, Qin P, Lapizco-Encinas BH et al., ACS applied materials & interfaces, 2020, 12, 7888–7896. [PubMed: 31939648]
45. Nanaware A, Kranbuhl T, Ching J, Chen JS, Chen X, Tu Q and Du K, Journal of Vacuum Science & Technology B, 2022, 40, 063002.
46. Hassoun A, Linden PK and Friedman B, Critical care, 2017, 21, 1–10. [PubMed: 28057037]
47. Cecconi M, Evans L, Levy M and Rhodes A, The Lancet, 2018, 392, 75–87.
48. Bao M, Zhang S, Ten Pas C, Dollery SJ, Bushnell RV, Yuqing F, Liu R, Lu G, Tobin GJ and Du K, Lab on a Chip, 2022, 22, 4849–4859. [PubMed: 36111877]
49. Yin J, Zou Z, Hu Z, Zhang S, Zhang F, Wang B, Lv S and Mu Y, Lab on a Chip, 2020, 20, 979–986. [PubMed: 32003380]
50. Lin M, Yue H, Tian T, Xiong E, Zhu D, Jiang Y and Zhou X, Analytical Chemistry, 2022, 94, 8277–8284. [PubMed: 35635176]

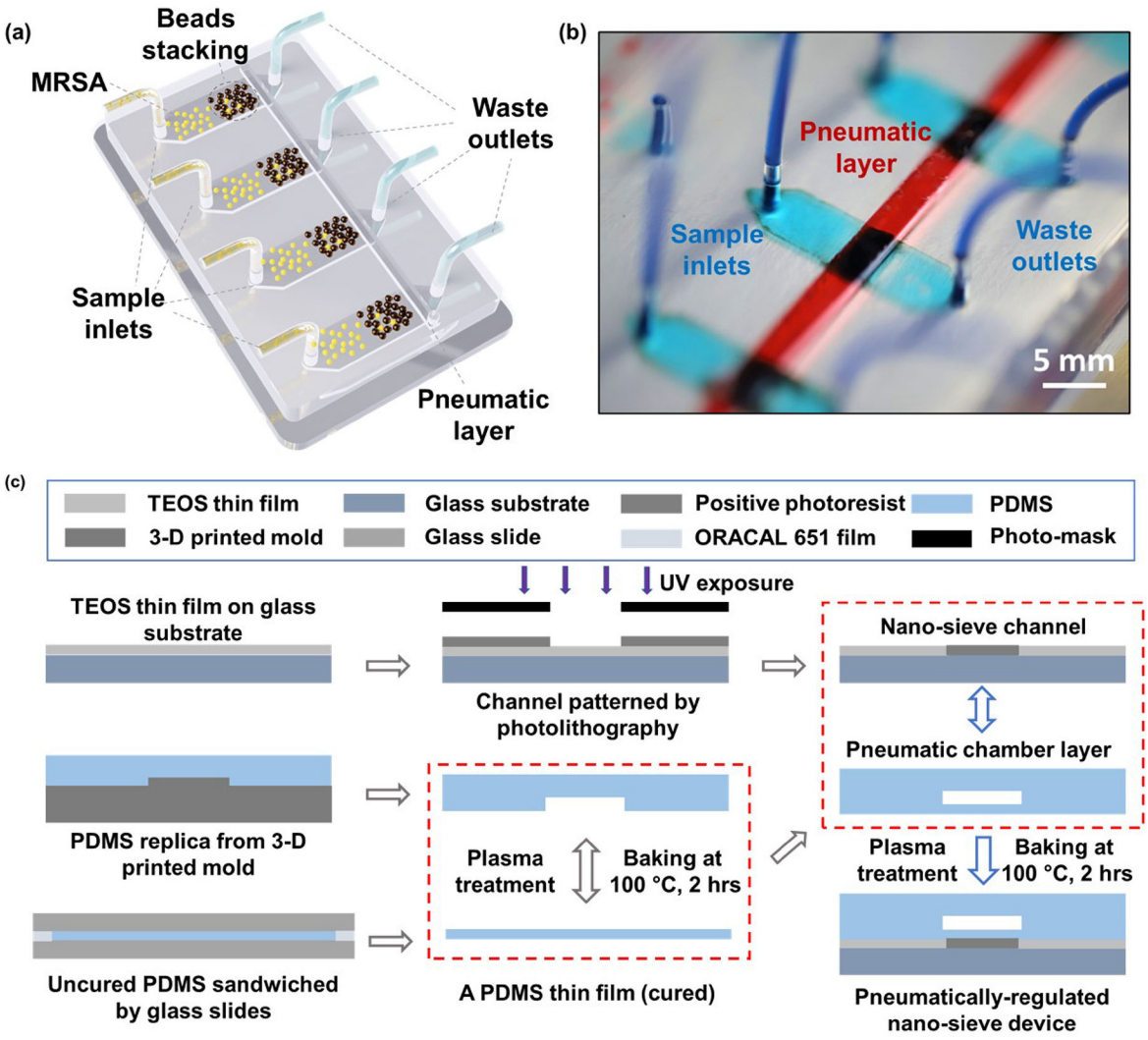

Fig. 1.

(a) Schematic of nano-sieve device. The MRSA sample is injected through sample inlets, and subsequently, bacteria become entrapped within the beads stacking region of the microfluidic channel, allowing for effective MRSA concentration. Meanwhile, the waste liquid, consisting of plasma and phosphate-buffered saline (PBS), exits the device through designated waste outlets. (b) Image of realized multi-channel nano-sieve with food dye. (c) Fabrication process of nano-sieve device.

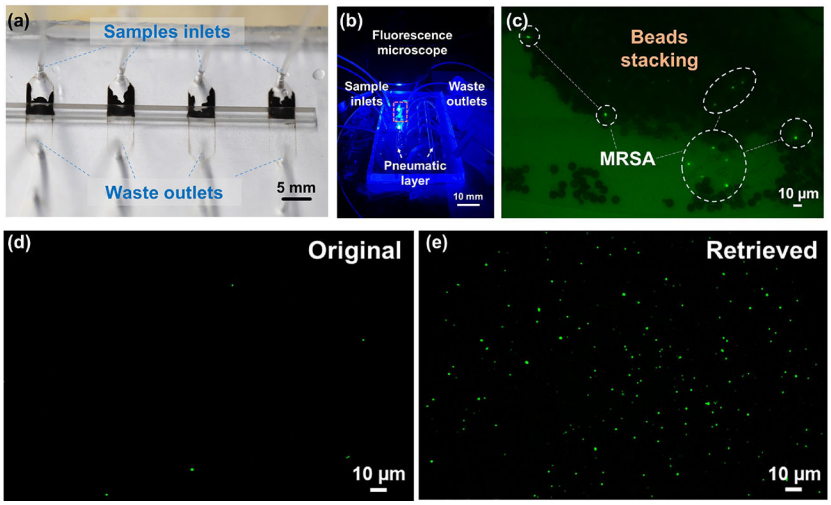

Fig. 2.

(a) Magnet beads pattern in the channel without MRSA. (b) Experimental setup of multiplexing separation of target bacteria under the fluorescence microscope. (c) Beads stacking with MRSA under fluorescence microscope. (d) The original bacterial sample and (e) retrieved bacterial sample were compared to indicate the on-chip concentration capability of the nano-sieve device.

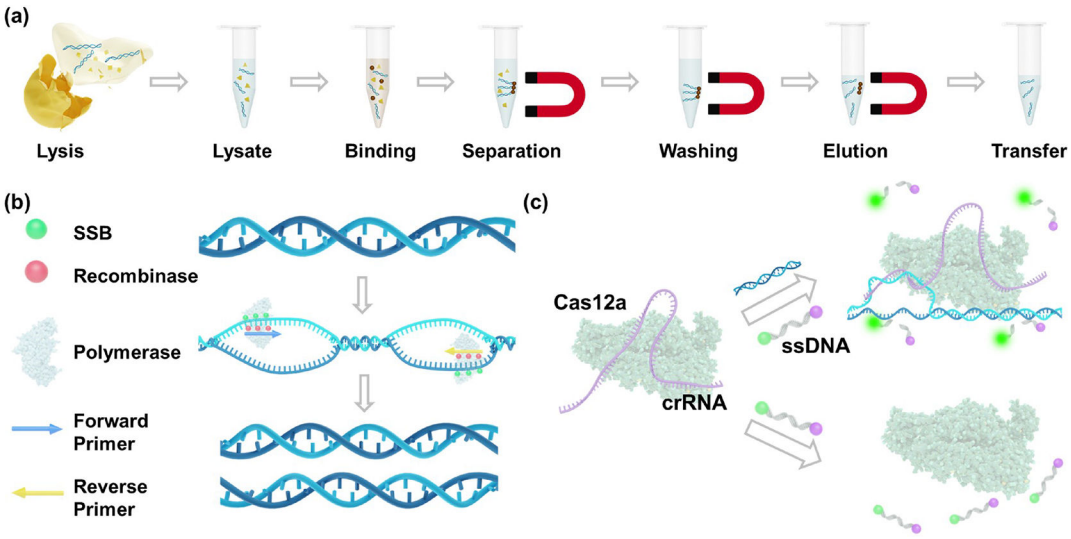

Fig. 3.

(a) Nucleic acid purification process using magnet beads after MRSA lysis. (b) Mechanism of RPA amplification. Recombinases assist in primer binding to target DNA, while SSB proteins stabilize the strands. Polymerases then use building blocks (dNTPs) to form new DNA strands. (c) Mechanism of CRISPR-Cas12a detection involving the formation of a Cas12a-crRNA-DNA complex and cleavage of the fluorophore-quencher probe.

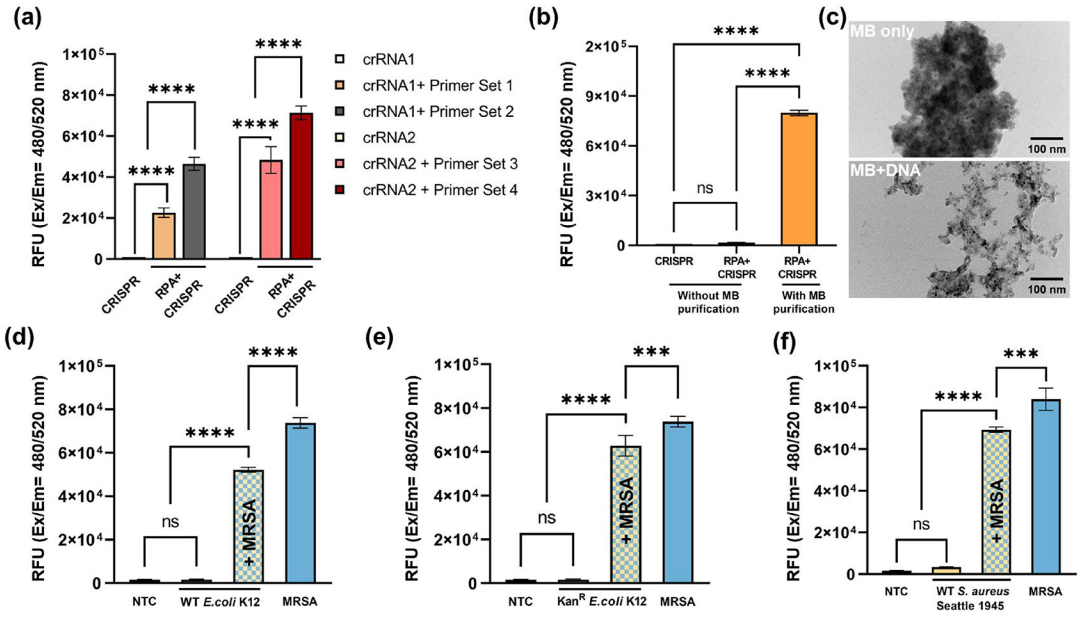

Fig. 4.

(a) Primer screening for RPA amplification. (b) MRSA detection with/without purification using magnet beads. (c) TEM images of magnet beads only (top) and magnet beads plus DNA (bottom), with a scale bar of 100 nm. (d), (e), and (f) represent the specificity tests of this assay using wild-type *E. coli* K12, kanamycin-resistant *E. coli* K12, and wild-type *S. aureus*, respectively. "NTC" refers to no template control. The data are represented as mean ± standard deviation ($n = 3$). For statistical analysis, *ns*, not significant = $p > 0.05$; *** = $0.0001 < p \leq 0.001$; **** = $p \leq 0.0001$.

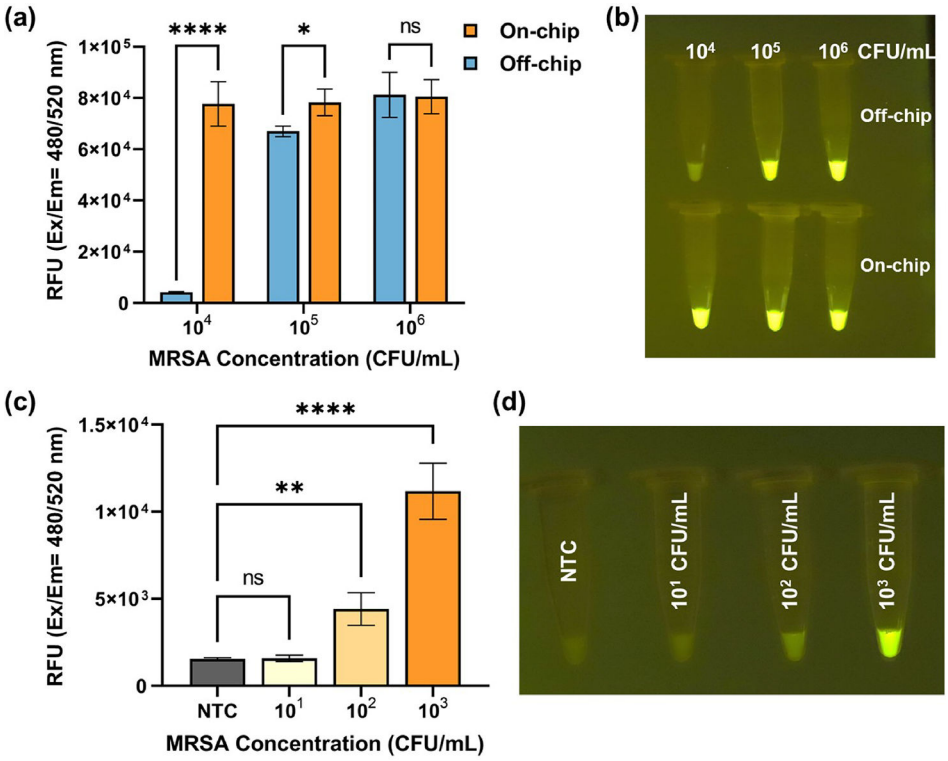

Fig. 5.

(a) Quantified fluorescence signal of off-chip and on-chip detection with varying inlet MRSA concentrations ranging from 10^4 CFU/mL to 10^6 CFU/mL (Ex/Em = 480/520 nm). (b) Endpoint images of the reactions excited by a transilluminator (wavelength: 465 nm) in response to different inlet MRSA concentrations ranging from 10^4 CFU/mL to 10^6 CFU/mL (excitation wavelength: 465 nm). (c) Quantified fluorescence signal of on-chip detection with inlet MRSA concentration ranging from 10 CFU/mL to 10^3 CFU/mL (Ex/Em = 480/520 nm). (d) Endpoint images of the reactions excited by a transilluminator (wavelength: 465 nm) in response to different inlet MRSA concentrations ranging from 10 CFU/mL to 10^3 CFU/mL. "NTC" refers to no template control. The data are represented as mean ± standard deviation ($n = 3$). For statistical analysis, *ns*, not significant = $p > 0.05$; * = $0.01 < p \leq 0.05$; ** = $0.001 < p \leq 0.01$; **** = $p \leq 0.0001$.

Table 1

Concentration factor of nano-sieve

Channel	Inlet Concentration (CFU/mL)	Outlet Concentration (CFU/mL)	Experimental Concentration Factor	Theoretical Concentration Factor
1	4.00×10^{2}	$(6.00\pm2.94)\times10^{3}$	15.00	20.00
2	5.93×10^{3}	$(8.47\pm1.07)\times10^{4}$	14.27	20.00
3	7.43×10^{4}	$(8.37\pm1.40)\times10^{5}$	11.26	20.00
4	3.43×10^{5}	$(4.07\pm0.60)\times10^{6}$	11.84	20.00
5	3.80×10^{6}	$(4.07\pm0.60)\times10^{7}$	10.79	20.00